NASA Technical Memorandum 100436

Surface Flow Visualization of Separated Flows on the Forebody of an F-18 Aircraft and Wind-Tunnel Model

David F. Fisher, David M. Richwine, and Daniel W. Banks

May 1988

NASA
National Aeronautics and
Space Administration

NASA Technical Memorandum 100436

Surface Flow Visualization of Separated Flows on the Forebody of an F-18 Aircraft and Wind-Tunnel Model

David F. Fisher, David M. Richwine, and Daniel W. Banks
Ames Research Center, Dryden Flight Research Facility, Edwards, California

1988

NASA
National Aeronautics and
Space Administration
Ames Research Center
Dryden Flight Research Facility
Edwards, California 93523-5000

SURFACE FLOW VISUALIZATION OF SEPARATED FLOWS ON THE FOREBODY OF AN F-18 AIRCRAFT AND WIND-TUNNEL MODEL

David F. Fisher*
NASA Ames Research Center
Dryden Flight Research Facility
Edwards, California

David M. Richwine*
PRC Kentron
Edwards, California

Daniel W. Banks*
NASA Langley Research Center
Hampton, Virginia

Abstract

A method of in-flight surface flow visualization similar to wind-tunnel-model oil flows is described for cases where photo-chase planes or onboard photography are not practical. This method, used on an F-18 aircraft in flight at high angles of attack, clearly showed surface flow streamlines on the fuselage forebody. Vortex separation and reattachment lines were identified with this method and documented using postflight photography. Surface flow angles measured at the 90° and 270° meridians, show excellent agreement with the wind tunnel data for a pointed tangent ogive with an aspect ratio of 3.5. The separation and reattachment line locations were qualitatively similar to the F-18 wind-tunnel-model oil flows but neither the laminar separation bubble nor the boundary-layer transition on the wind tunnel model were evident in the flight surface flows. The separation and reattachment line locations were in fair agreement with the wind tunnel data for the 3.5 ogive. The elliptical forebody shape of the F-18 caused the primary separation lines to move toward the leeward meridian. Little effect of angle of attack on the separation locations was noted for the range reported.

Nomenclature

AEDC 16T	Arnold Engineering Development Center 16T Wind Tunnel
C_l	rolling moment coefficient
$C_{L_{max}}$	maximum lift coefficient
d	forebody maximum diameter, 49.3 in., full scale
h	height of forebody, in.
l	length of forebody, 123.5 in., full scale
LEX	leading edge extension
LSB	laminar separation bubble
m.a.c.	mean aerodynamic chord, 138.3 in., full scale
PGME	propylene glycol monomethyl ether
R	reattachment line location
Re_c	Reynolds number based on mean aerodynamic chord
Re_d	Reynolds number based on forebody maximum diameter
$S1$	primary vortex separation line location
$S2$	secondary vortex separation line location
V_∞	freestream velocity
w	width of forebody, in.
x	distance from nose apex, in.
α	aircraft angle of attack, deg
α'	forebody angle of attack ($\alpha' = \alpha - 5.6°$), deg
β	aircraft angle of sideslip, deg
ϕ	aircraft roll angle, deg
θ	angle measured clockwise from windward meridian, deg

Introduction

It is well known that forebody flow characteristics can strongly affect the stability and control characteristics of modern fighter aircraft at high angle of attack. Ground-based wind tunnel studies have resulted in anomalies with respect to forebody flow characteristics. For example, during the early wind tunnel tests of F-18 models, a discrepancy appeared between the small scale (6-percent model) high Reynolds number results and the larger scale (16-percent model) low Reynolds number results. While the directional stability results from the two models were in agreement, the lateral stability results were not. The data from the 16-percent model in the NASA Langley 30 by 60-Foot Tunnel showed a lateral instability between 30° and 40° angle of attack, that is, near-maximum lift coefficient $C_{L_{max}}$, while the 6-percent model tested in the Arnold Engineering Development Center 16T Wind Tunnel (AEDC 16T) and the NASA Ames 12-Foot Pressure Wind Tunnel at high Reynolds number both indicated stable lateral stability. Consequently, it was felt that the high Reynolds number 6-percent model data was of higher quality and hence, the 16-percent model results were not believed.

Later, during the flight testing of the F/A-18 aircraft, a mild yaw departure occurred. While attempting a windup turn, the angle of attack exceeded 30°, and the sideslip angle was 15° at Mach 0.7. Analysis of the flight data revealed yawing and rolling moment coefficients that agreed well with the previous 16-percent model low Reynolds number results, as shown in Fig. 1.[1]

*Aerospace engineer. Member AIAA.

In an effort to determine the reason for the discrepancy in the 6-percent model results, the 6-percent high Reynolds number scale model, 7-percent scale model, and 16-percent scale model were tested in the 30 by 60-Foot Tunnel.[1] Each model was tested at the same Reynolds number based on wing chord. Results from both the 6-percent and the 7-percent scale model from the 30 by 60-Foot Tunnel compared well with the high Reynolds number wind tunnel data previously obtained at Ames and AEDC, hence, ruling out a facility effect. Geometric parameters that could affect the vortex interactions from the forebody, leading edge extension (LEX), and wing were investigated using the 7-percent and 16-percent models. Some of the geometric parameters investigated were forebody on/off, LEX on/off, LEX boundary-layer bleed slots open/closed, and radome strake on/off.

To provide a realistic assessment of the incremental forebody effects on lateral stability at high angles of attack, the fuselage forebody was removed and replaced with a fairing. The results of these tests[1] indicated that removing the forebody on the 16-percent model showed little difference in the rolling moment coefficient. Removing the forebody of the 7-percent model produced a large change in the rolling moment coefficient, with the resulting lateral stability in agreement with the 16-percent model. Reference 1 suggested that the apparent model-scale sensitivity encountered in these tests was associated with different boundary-layer separation line locations on the fuselage forebody and the forebody vortices interaction with the LEX-wing flowfield.

In order to investigate the problems of high angle of attack on fighter aircraft, NASA has established the high alpha test program (HATP) using in part the F-18 high alpha research vehicle (HARV; Fig. 2). One part of the HATP was the further investigation of this model-scale anomaly of lateral stability. Both flow visualization and pressure distributions of the separated flows on the forebody and LEXs were planned. It was desirable to obtain surface flow visualization data in flight comparable to wind tunnel model oil flows. Several methods, such as tufts or oil flows,[2,3] were considered, but both required a chase aircraft flying in close proximity to the test aircraft. With the test aircraft flying at 20° to 50° angle of attack or higher at very low airspeeds and with little lateral stability, it did not seem prudent to have another aircraft flying nearby. Onboard cameras could provide good documentation of tufts or oil flows but require good, nearly perpendicular, viewing angles. For the F-18 forebody, these viewing angles were not available. Another method that could document the flow between test points or after each flight was required.

One method that looked promising was used in Refs. 4 and 5. A liquid with dye was emitted from tubes laid on the aft fuselage skin of an MD-80 and allowed to dry at a given flight condition. Surface flow streamlines were then identified and documented using postflight photography. This method was adapted for use on the F-18 forebody. The design of the surface flow visualization system is presented, along with preliminary results achieved during flight test of the F-18 HARV to angles of attack between 19° and 47°.

Vehicle Description

The high alpha research vehicle (HARV) is a single-place F-18 aircraft powered by two F404-GE-400 turbofan engines with afterburner. The aircraft features a variable-camber midwing with leading edge extensions (LEX) mounted on each side of the fuselage extending forward of the wing roots to just forward of the windshield. The F-18 HARV is flown by NASA in the clean configuration, without stores and uses flight control computers with the 8.3.3 PROM set. The aircraft has an unrestricted angle-of-attack flight envelope in this configuration, with a center of gravity between 17-percent and 25-percent mean aerodynamic chord (m.a.c.).

F-18 Forebody Geometry

The F-18 forebody from the nose apex to the canopy consists of an ogive nosecone with a circular cross-sectional shape blending into a fuselage having an oblate elliptical, cross-sectional shape. The longitudinal axis of the nosecone is depressed 5.6° with respect to the waterline of the aircraft. The noseboom attached to the nosecone at the apex is 5.8 ft long and is parallel with the waterline of the aircraft. Flush surface orifices were installed at five fuselage stations on the forebody for surface flow visualization and pressure measurements. The first three rows of orifices are located on the circular cross-sectional shape (Fig. 3), whereas the last two orifice rows are on the oblate elliptical cross-section of the forebody. The fuselage height-to-width ratios h/w at these two locations are 1.10 and 1.35 for $x/l = 0.66$ and $x/l = 1.0$, respectively. The aspect ratios of the forebody from the top and side views are shown in Fig. 3. The aspect ratio of the side view l/h is 2.5, while the aspect ratio of the top view l/w is 3.4. For comparison, the shape of the pointed 3.5 tangent ogive shape of Ref. 6 is also shown.

F-18 Forebody Flowfield

The flow field about the F-18 at high angle of attack is dominated by three-dimensional separated flow from the LEXs and forebody. Strong vortices form from the sharp-edged LEXs while somewhat weaker vortices roll up from the forebody, as shown in Fig. 4 from a water tunnel study of Refs. 7 and 8. At high angle of attack, the flow about the forebody of the F-18 is similar to that of an ogive or cone.[6,9] Figure 5 shows symmetrical separation where the flow about the forebody splits at the stagnation point on the windward side, sweeps around the forebody, separates at point $S1$ on the leeward side, and rolls inboard into a pair of primary vortices. The primary vortices induce a secondary flow field that consists of a pair of secondary vortices that separate at $S2$ and are of opposite rotation to the primary vortices. At zero sideslip, these vortices can be symmetrical or asymmetrical[6] and can generate significant levels of side force. Points R in Fig. 5 are where the flow re-attaches to the forebody.

Surface Flow Visualization System

A plumbing schematic of the surface flow visualization system is shown in Fig. 6. Propylene glycol monomethyl ether (PGME)

and a toluene-based dye were used as the fluid medium, as demonstrated in Refs. 4 and 5. The PGME/dye reservoir shown is a hydraulic accumulator with an internal piston commonly used in aircraft hydraulic systems. Block valves were used to turn the flow to each orifice on and off. Each block valve permitted 32 fluid lines to be turned on or off at a time. Six block valves were required for the 192 orifices used. Each outgoing line was connected to a single surface orifice with nylon tubing. At each 0.046-in.-diameter surface orifice, an inline 0.020-in.-diameter restrictor was used both to help limit the fluid flow while the system was operating and to retain the fluid in the line after the system was shut off.

The purpose of the block valves was to prevent fluid from bleeding back from an orifice on top of the forebody through the manifold and out an orifice on the bottom of the forebody after the system was shut off. The block valves used in this experiment are ESP-32 calibration valves normally used for gases with 32 lines coming in and 32 lines going out. These valves were modified with a replacement face plate and a manifold fed by one 1/4-in.-diameter line shown in Fig. 7. The valve is operated by applying pressure to orifice C1 to slide the block in the closed position or to orifice C2 to slide the block to the open position.

Before each flight, the F-18 forebody was cleaned with denatured alcohol. Where possible, joints and seams were filled with a silicon sealer. The PGME/dye mixture was loaded into the hydraulic accumulator and the system primed to the block valves. When the aircraft reached the desired test altitude, usually about 20,000 to 25,000 ft, the N2 and PGME/dye shutoff valves were opened to pressurize the accumulator. After the pilot had stabilized the aircraft at the desired high-α conditions, he pulled and held the trigger on the control stick. This opened the block valves to release the fluid through the flush orifices on the surface of the forebody. He then released the trigger approximately 15 sec later to close the block valves. The test conditions were then held for another 60 sec to allow the PGME to evaporate and the dye to "dry." Approximately 1 qt of liquid was used at each test point.

Note of caution: PGME is flammable and should be treated as a fuel. It is not compatible when in constant contact with many materials. The extent of compatibility should be checked before use, especially with "O" rings and seals. Areas where the duration of contact with the PGME fluid was short, such as the aircraft skin, paint, and canopy, the fluid was not a problem other than some minor paint staining. The system should be purged after each use to limit system exposure to the PGME/dye fluid and to prevent residue buildup from the dye within the system.

One surface flow visualization test point was obtained per flight with this method. The surface flow visualization test points were scheduled to be the last test point of each flight before returning to base so that the dye on the surface which had not completely dried would not be contaminated or smeared later during the flight. Nonchlorinated Bon Ami was not used as a dye absorbent,[4,5] as this tended to blur the surface flow streamlines. Photos were taken after the flight to document the surface flow streamlines. The aircraft was cleaned with denatured alcohol or clear PGME fluid within several hours after each flight. If cleaning does not occur within several hours after each flight, staining of the aircraft surface may occur.

Results

Surface flow visualization data from the F-18 HARV were obtained at angles of attack from 19° to 47°. Sample time histories of the flight conditions are shown in Fig. 8. At time = 0, the PGME/dye mixture is released on the surface for approximately 15 sec. The pilot then attempts to hold the test conditions constant for a minute to allow the PGME to flow, evaporate, and the dye to set up or "dry" on the aircraft surface. As can be seen in Fig. 8(a), at angle of attack $\alpha = 30°$, the pilot could hold α to within $\pm 0.75°$ with the angle of sideslip β $\pm 1.5°$. However at $\alpha = 37°$, a slow wing rock developed, as can be seen by the roll angle ϕ. This is due to the low lateral stability of the F-18 at this angle of attack. While the angle of attack could be held to $\pm 1.5°$, the angle of sideslip varied from $-5.5°$ to $+11°$ and was in phase with the roll angle.

In-flight photos of PGME/dye emitting from the forebody static orifices are shown in Fig. 9. The photos were taken with a 35 mm camera mounted in a wingtip pod. The photos were taken at approximately 4.7, 6.5, and 11.3 sec after the trigger was pulled and the fluid flow was initiated. The PGME/dye is first observed emitting from the first, second and third orifice rings on the nosecone (Fig. 9(a)) and out the fourth and fifth orifice rows (Fig. 9(b)) about 2 sec later. In Fig. 9(c), the PGME/dye is observed traveling down the primary vortex separation line on the forebody.

An example of surface flow visualization on the F-18 forebody for an $\alpha = 34°$ is shown in the postflight photos of Fig. 10. The remaining dye from this technique clearly showed the surface flow streamlines. Where the surface streamlines merge, the flow lifted from the surface and rolled up into a vortex core. Along the streamlines where the flow merged, the separation lines for the vortices were defined. The primary and secondary vortex separation lines can be readily identified.

As a comparison to the flight surface flow visualization technique, an oil flow from the 16-percent scale model in the LaRC 14- by 22-Foot Subsonic Tunnel is shown in Fig. 11(a) at $\alpha = 36°$. In this case, the model was painted a smooth gloss black, and white titanium dioxide mixed in mineral oil with a small amount of oleic acid added to aid in dispersion was brushed onto the model surface. The flow pattern on the model appears to be predominantly laminar. The separation line that extends from the apex of the nose rearward appears to be a laminar separation bubble. A laminar separation bubble is itself a small vortex that scrubs the surface and pumps the oil mixture downstream, creating the black void region seen in Fig. 11(a). On the forward, circular part of the nose, the flow seems to re-attach temporarily and then immediately separates where the pooling is seen, just past the separation bubble itself, forming the primary vortex. Further back on the nose, where the cross section is more elliptical, flow re-attaches across the laminar separation bubble in what appears to be turbulent or transitioning flow. At the top of this turbulent region is the primary vortex separation line where the flow separates and forms the primary vortex. The secondary separation line is not as well defined but is the dark void region above and inboard of the primary separation line.

The most obvious difference between the wind tunnel and flight surface flow visualization is the laminar separation bubble and transition to turbulent flow seen in the wind tunnel oil flows and

not observed in the flight surface flow visualization. The wind tunnel tests were run at a Reynolds number based on the forebody maximum diameter of 0.32×10^6 for the 16-percent model, whereas the flight data was obtained at a Reynolds number of 3.9×10^6. The 16-percent model Reynolds number is near the critical Reynolds number for cylinders at angle of attack,[10] and transition would be expected to occur longitudinally along the model. In Fig. 11(b), the pressure distribution at $x/l = 0.39$ for this model at the same conditions is shown. The circumferential angle θ is measured clockwise looking aft about the longitudinal axis of the forebody with 0° (360°) the windward meridian and 180° the leeward meridian. The laminar separation bubble (LSB) and primary vortex separation line ($S1$) locations from the wind tunnel oil flows are shown. As can be seen, the LSB forms at the onset of the adverse pressure gradient. Transition occurs shortly thereafter and the boundary layer separates from the surface at $S1$ to form the primary vortex. In flight, the Reynolds number is much higher, and no evidence of transition is seen in the photos in Fig. 10. The discontinuity at the intersection of the 4-in.-diameter noseboom and nose apex on the aircraft most likely trips the boundary layer from laminar to turbulent flow. With transition at the nose apex at this Reynolds number and angle of attack, the calculated attachment line momentum thickness Reynolds number,[11] is greater than 100. This implies that a turbulent attachment line boundary layer is present along the windward meridian, and hence, the boundary layer on the forebody is turbulent.

Another example of the in-flight surface flow visualization technique at a lower angle of attack is shown in Fig. 12. At $\alpha = 19°$, the beginning of vortex flow on the F-18 forebody is shown where the surface flow streamlines converge. At this angle of attack, however, the secondary vortex separation line is not evident.

The surface flow angles on the forebody were measured from side view photos at $\theta = 90°$ and 270°, as shown in Fig. 13. Measurements were made at three forebody stations, $x/l = 0.20, 0.39$, and 1.0. All surface flow measurements were taken with respect to the forebody longitudinal axis which is depressed 5.6° from the aircraft longitudinal axis. The surface flow angles measured are shown as a function of forebody angle of attack α' in Fig. 14. The data shows excellent agreement with the data for the 3.5 ogive of Ref. 6. Also shown in this figure is the boundary layer edge streamline for potential flow and a curve from Ref. 6 for flow very near an ogive apex. The surface streamline flow angles for $x/l = 0.39$ agree well with the potential flow curve. The surface streamline flow angles for $x/l = 0.20$ are higher than the potential flow curve and for the data at $x/l = 0.39$, as expected, due to the smaller body radius and transverse pressure gradient. The surface streamline flow angles from $x/l = 1.0$ show the influence of the LEX flow field. At $\alpha' = 13°$, the surface flow streamline angle is less than the potential flow prediction. At this angle of attack, the flow for the 90° and 270° meridian flow beneath the LEX leading edge. At $\alpha' = 32°$, the surface flow streamline flow angle is much higher than the potential flow curve, and the surface streamlines are pulled over the LEX leading edge by the powerful LEX vortex.

The separation and re-attachment locations for the primary and secondary vortices at $x/l = 0.66$ and 1.0 from flight are given in Fig. 15. In Fig. 15(a) the separation and re-attachment locations are shown as a function of h/w. At both of these locations the forebody cross section is no longer circular. The geometry of the forebody moves the separation locations on the more elliptical location toward the leeward meridian. Also shown in the figure are separation and re-attachment locations for a circular cross section 3.5 ogive at $\alpha' = 25°$ to 30° from Ref. 6. As expected, due to the forebody geometry, the primary vortex separation lines at $x/l = 0.66$ show better agreement with the wind tunnel data than the data at $x/l = 1.0$. However, the secondary separation lines from $x/l = 1.0$ show slightly better agreement with the data of Ref. 6 than the data at $x/l = 0.66$.

In Fig. 15(b) the same data is shown as a function of angle of attack. At the angles of attack shown, the flight separation locations show little movement with angle of attack but do have slight asymmetry. The primary vortex separation lines at $x/l = 0.66$ show good agreement with the wind tunnel at the higher angles of attack. The secondary vortex separation lines at $x/l = 1.0$ agree well with the data of Ref. 6.

Concluding Remarks

A method of in-flight flow visualization similar to wind tunnel oil flows has been described for cases where photo-chase planes or onboard photography are not practical. This method used on an F-18 aircraft in-flight at high angles of attack clearly showed surface flow streamlines. Vortex separation and re-attachment lines were identified with this method at angles of attack from 19° to 37°.

The surface flow angles measured at the 90° and 270° meridian show excellent agreement with the wind tunnel data for a 3.5 ogive of Ref. 6. The separation and reattachment line locations looked qualitatively similar to F-18 16-percent model wind tunnel oil flows. The laminar separation bubble and boundary layer transition that occurred on the wind tunnel model were not evident in the flight surface flows as expected.

The separation and reattachment line locations were in fair agreement with the data for the 3.5 ogive of Ref. 6. The elliptical forebody shape of the F-18 caused the primary separation lines to move toward the leeward meridian. Little effect of angle of attack on the location of separation lines was noted for the range reported.

Future Plans

Plans are now in work to continue the surface flow visualization technique on the F-18 HARV. It is known from wind tunnel oil flows that the noseboom affects the forebody vortices development. This will be explored in flight using surface flow visualization during flight-testing of the F-18 HARV with the noseboom removed. Future flights will also include surface flow visualization on the LEX to identify and document the lines of separation and re-attachment there.

Later in the flight program, surface static pressures will be measured on the forebody and LEXs using the same orifices used for the flow visualization technique. The pressures will be integrated and forces and moments from these components calculated. In ad-

dition, using the obstacle block technique described in Refs. 9, 12, and 13, lines of separation and re-attachment can be determined at the orifice stations for comparison to the flight and wind tunnel results. It is hoped that these results and comparisons to similarly planned wind tunnel data will help explain the apparent model scale differences described in the Introduction. In addition, these results will be used to develop better computational fluid dynamics prediction methods.

References

[1] Erickson, G.E.: Water Tunnel Flow Visualization and Wind Tunnel Data Analysis of the F/A-18—Leading Edge Extension Vortex Effects. NASA CR-165859, 1982.

[2] Curry, R.E.; Meyer, R.R., Jr.; and O'Conner, M.: The Use of Oil for In-Flight Flow Visualization. NASA TM-84915, 1983.

[3] Crowder, J.P.: Flow Visualization Techniques Applied to Full-Scale Vehicles. AIAA-87-2421, 1987.

[4] Belevtsov, N.; Brumby, R.E.; and Hughes, J.P.: In-Flight Flow Visualization—A Fluid Approach. Society of Flight Test Engineers, 14th Annual Symposium Proceedings, Aug. 1983, pp. 4.2-1 to 4.2-7.

[5] Hughes, J.P.; Brumby, R.E.; and Belevtsov, N.: Flow Visualization From the Ground Up. AIAA-83-2691. 1983.

[6] Keener, E.R.: Flow-Separation Patterns on Symmetric Forebodies. NASA TM-86016, 1986.

[7] Lan, C.E. and Lee, I.G.: Investigation of Empennage Buffeting. NASA CR-179426, 1987.

[8] Wentz, W.H., Jr.: Vortex-Fin Interaction on a Fighter Aircraft. AIAA-87-2474, 1987.

[9] Peake, D.J.; Fisher, D.F.; and McRae, D.S.: Flight Experiments with a Slender Cone at Angle of Attack. AIAA-81-0337, 1981.

[10] Ericsson, L.E. and Reding, J.P. : Asymmetric Vortex Shedding From Bodies of Revolution, in *Tactical Missile Aerodynamics*, vol. 104. Hemsch, M.J. and Nielson, J.N., eds, 1986, pp. 243–296.

[11] Pfenninger, W.: Flow Phenomena at the Leading Edge of Swept Wings. Recent Developments in Boundary Layer Research, Part IV. AGARDograph 97, May 1965.

[12] Nituch, M.J.: The Use of Congruent Obstacle Blocks for the Indirect Measurement of Turbulent Skin Friction on Smooth Surfaces. Master's thesis, Carleton University (Ottawa), Aug. 1972.

[13] Elfstrom, G.M.; Kostopoulos, C.; Peake, D.J.; and Fisher, D. F.: The Obstacle Block as a Device to Measure Turbulent Skin Friction in Compressible Flow. AIAA-82-0589, 1982.

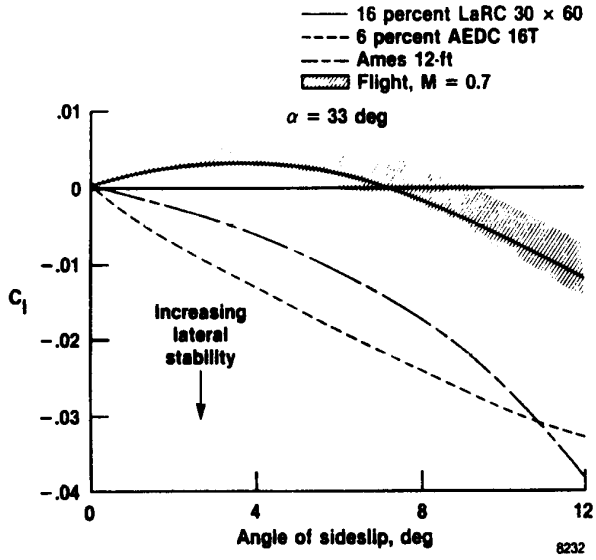

Fig. 1 Comparison of wind tunnel and flight rolling moment coefficients.

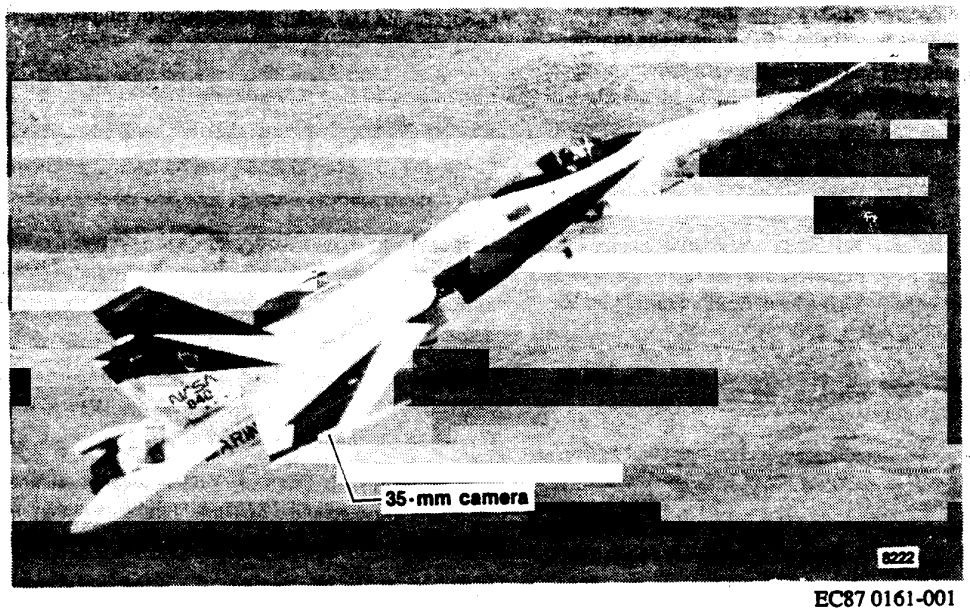

EC87 0161-001

Fig. 2 NASA F-18 high alpha research vehicle (HARV).

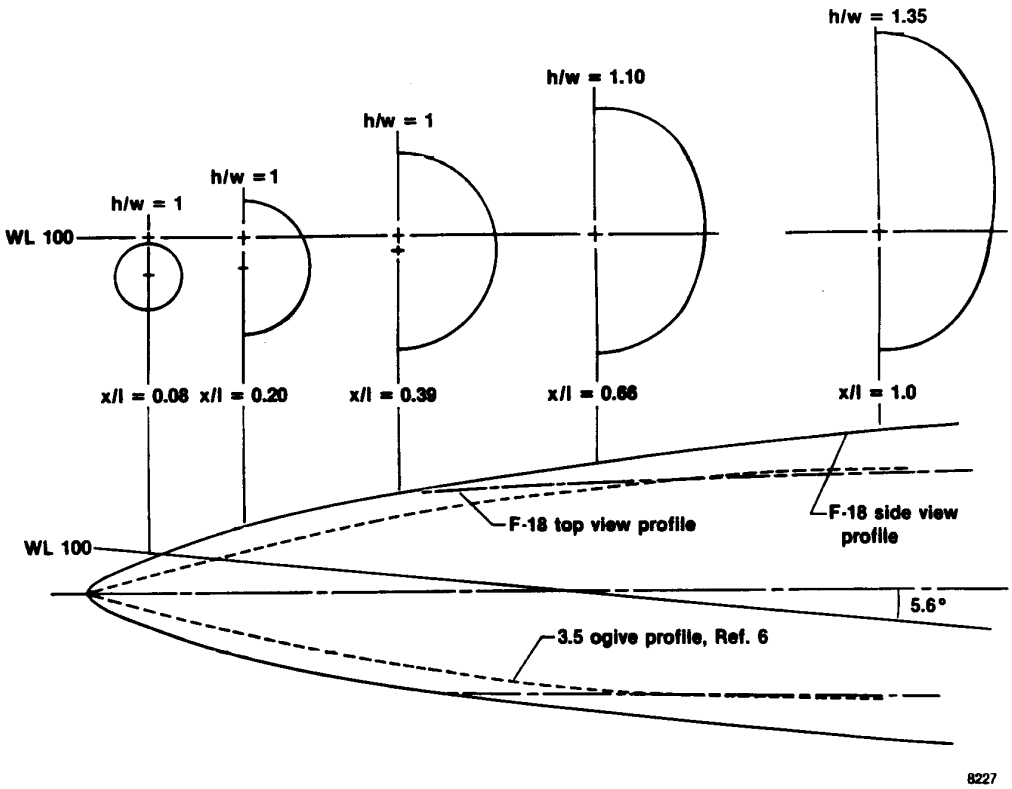

Fig. 3 F-18 forebody geometry.

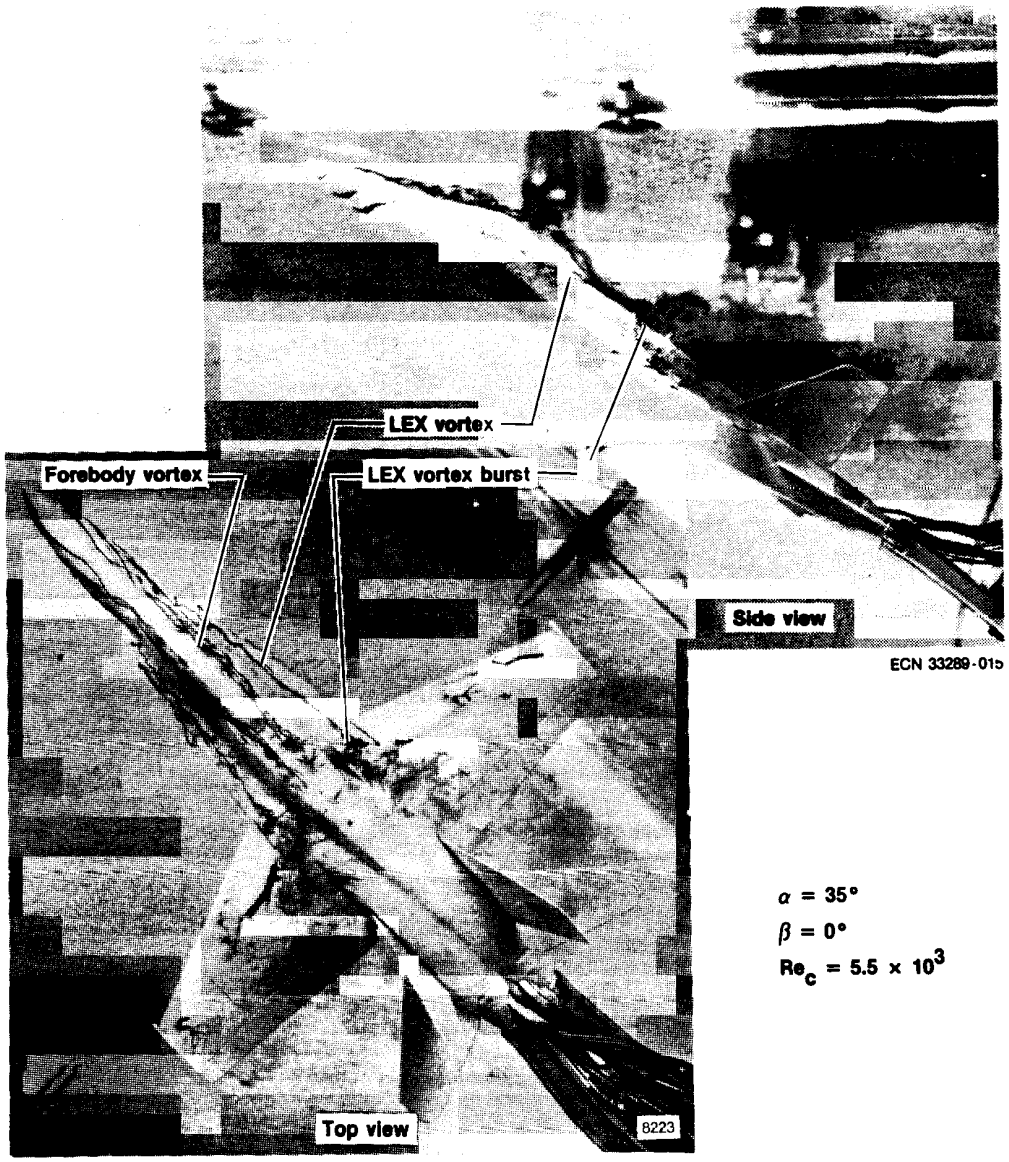

Fig. 4 Vortex flow on 1/48 scale F-18 model in DFRF water tunnel, $\alpha = 35°$.

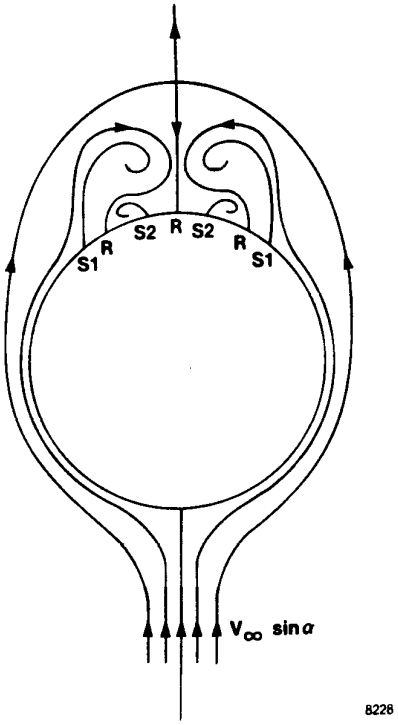

Fig . 5 Model of flow about forebody, symmetric flow (cross-sectional view).

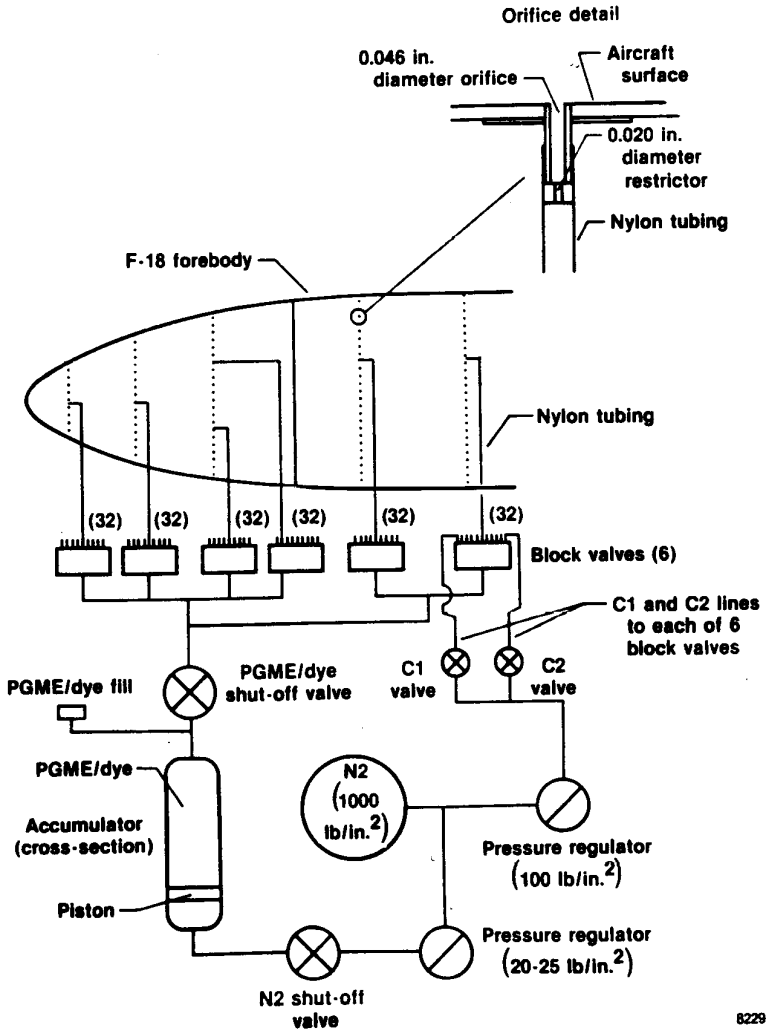

Fig. 6 Schematic of F-18 surface flow visualization system.

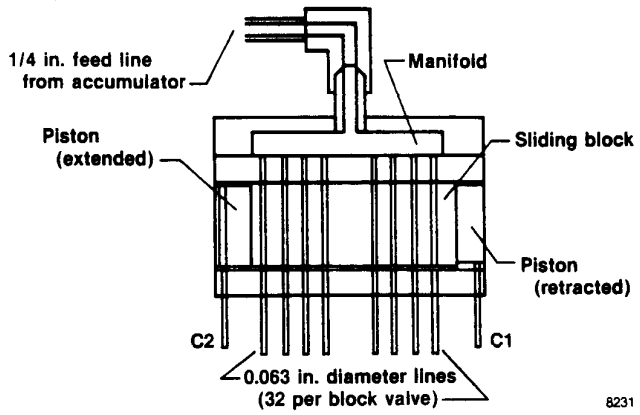

(a) Cross-sectional view.

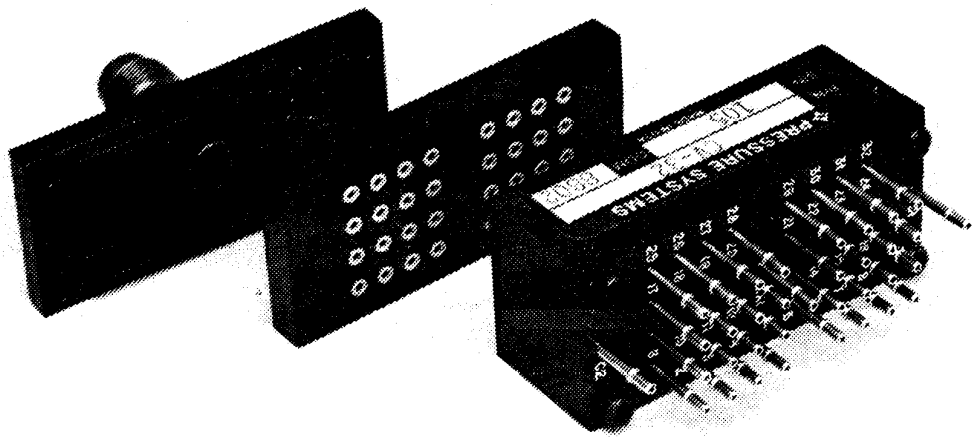

EC88 0003-001

(b) Isometric view of assembly.

Fig. 7 Modified block valve for surface flow visualization system.

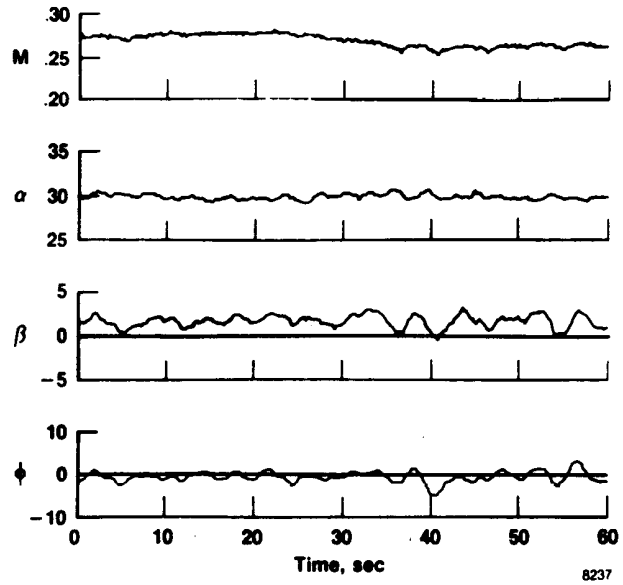

(a) $\alpha = 30°$.

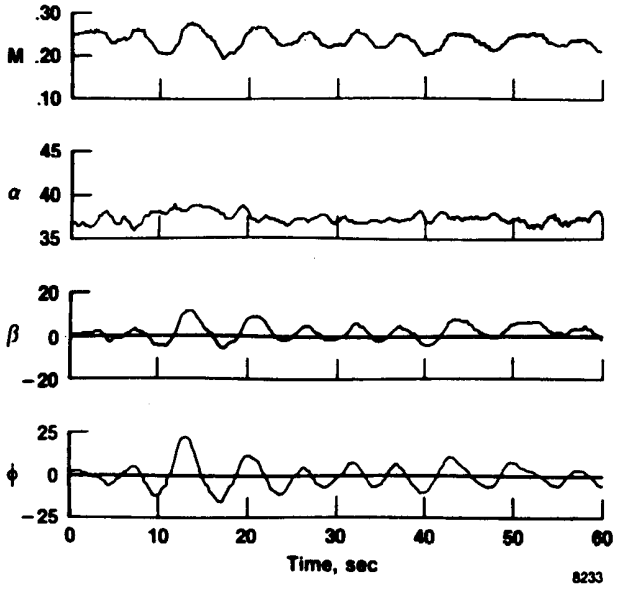

(b) $\alpha = 37°$.

Fig. 8 Surface flow visualization test parameter time history.

EC88 0010-004

(a) Surface flow 4.1 seconds after flow initiation.

EC88 0010-002

(b) Surface flow 6.5 seconds after flow initiation.

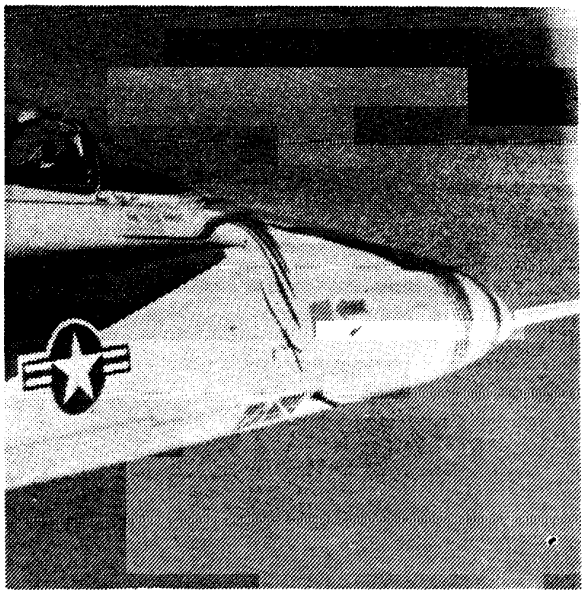

EC88 0010-008

(c) Surface flow 11.3 seconds after flow initiation.

Fig. 9 Photographs of in-flight operation of the F-18 surface flow visualization system.

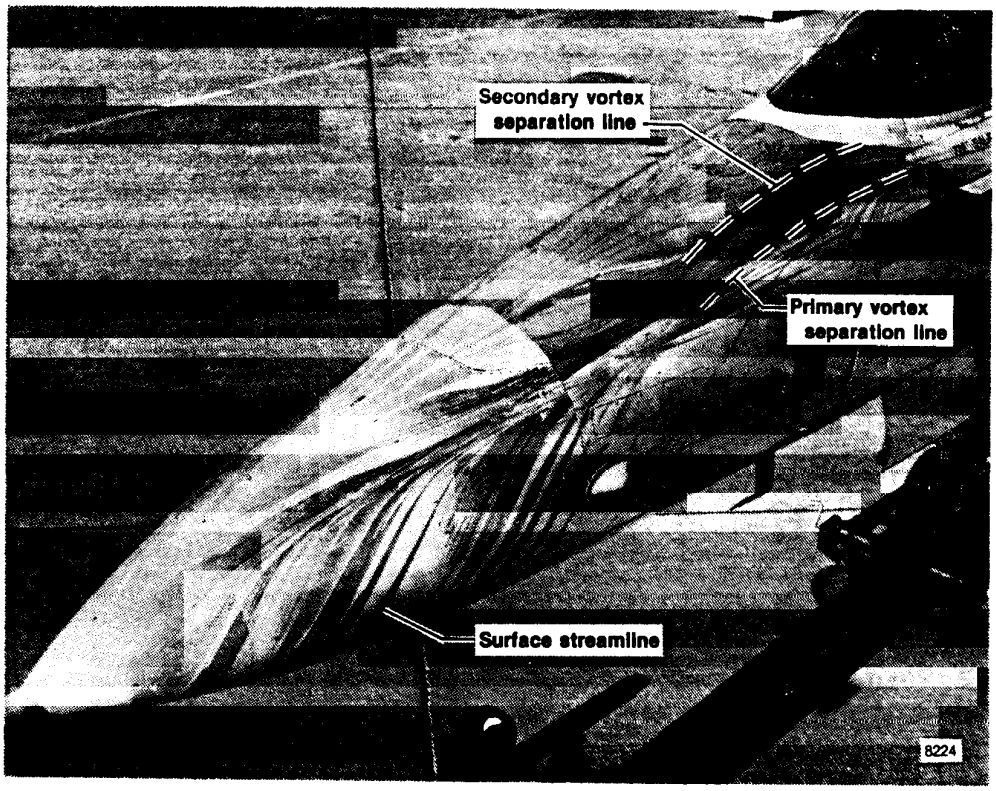

EC87 0277-007

(a) 1/4 view of forebody.

Fig. 10 Visualization of surface streamlines and lines of separation on F-18 forebody, $\alpha = 34°$.

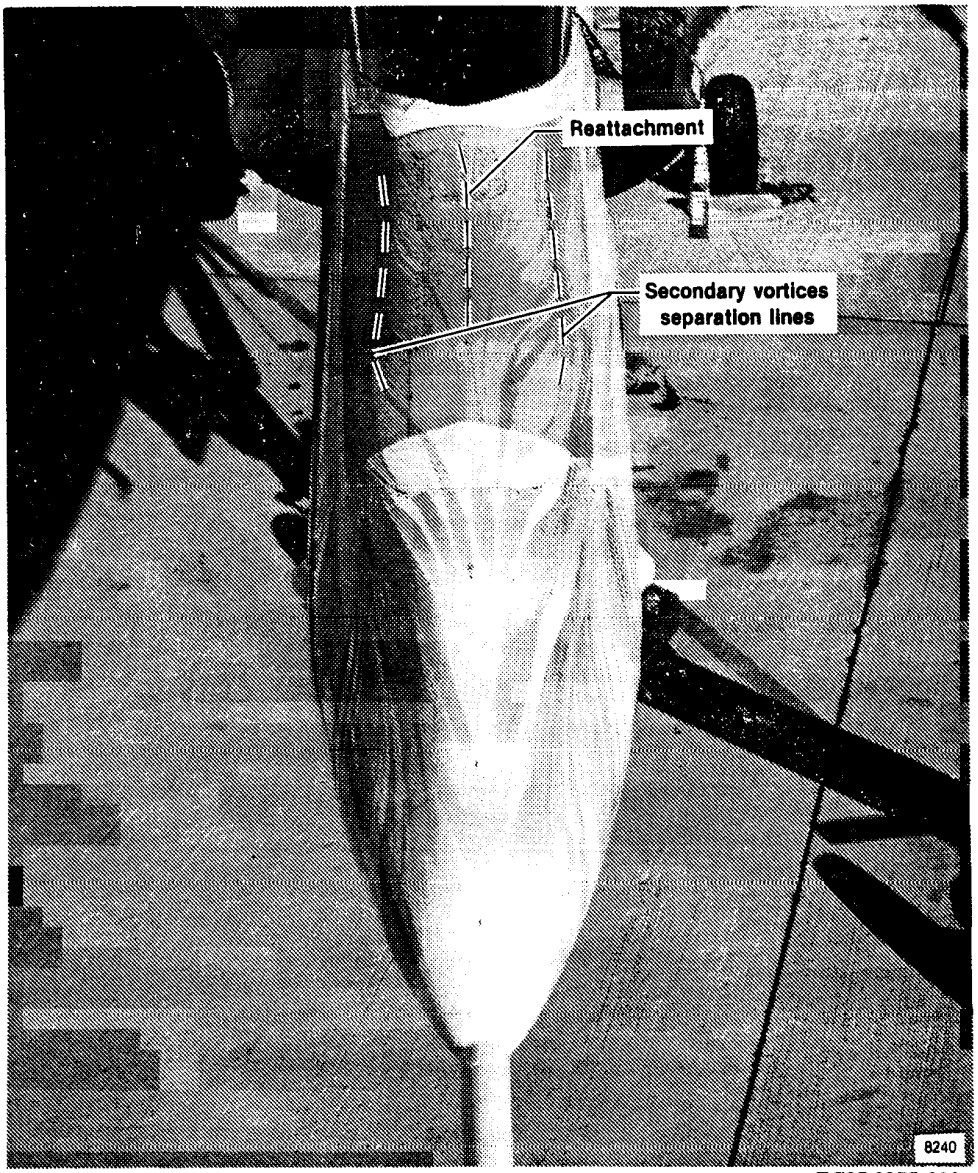

EC87 0277-008

(b) Head-on view of forebody.

Fig. 10 Concluded.

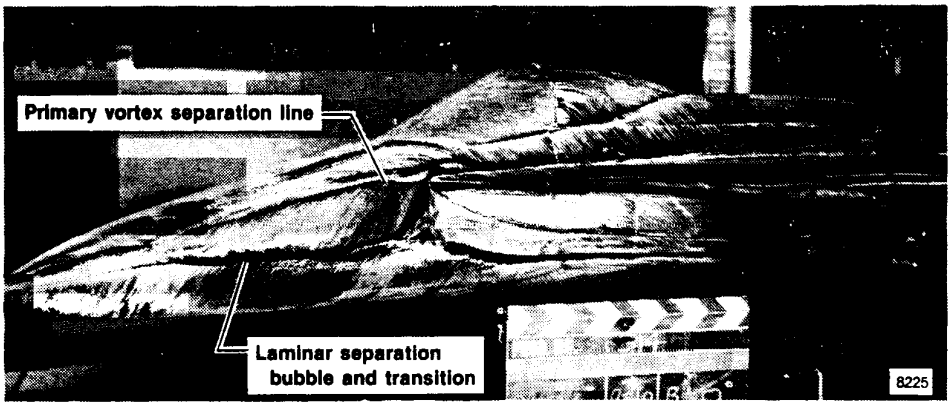

(a) Oil flow visualization of surface streamlines, LaRC photo.

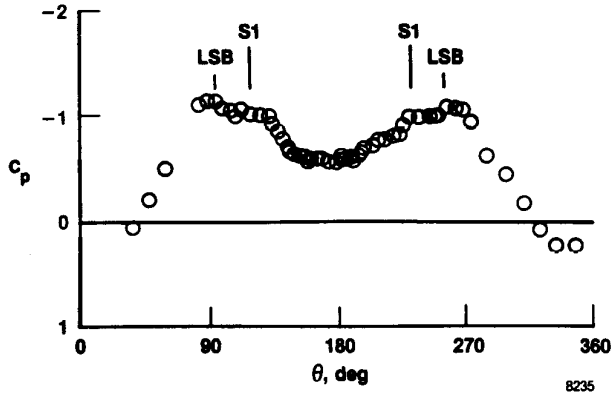

(b) Forebody circumferential pressure distribution, x/l = 0.39.

Fig. 11 Wind tunnel oil flow visualization and pressure distribution from 16 percent scale F-18 wind tunnel model, noseboom on, $\alpha = 36°$, $\beta = 0°$.

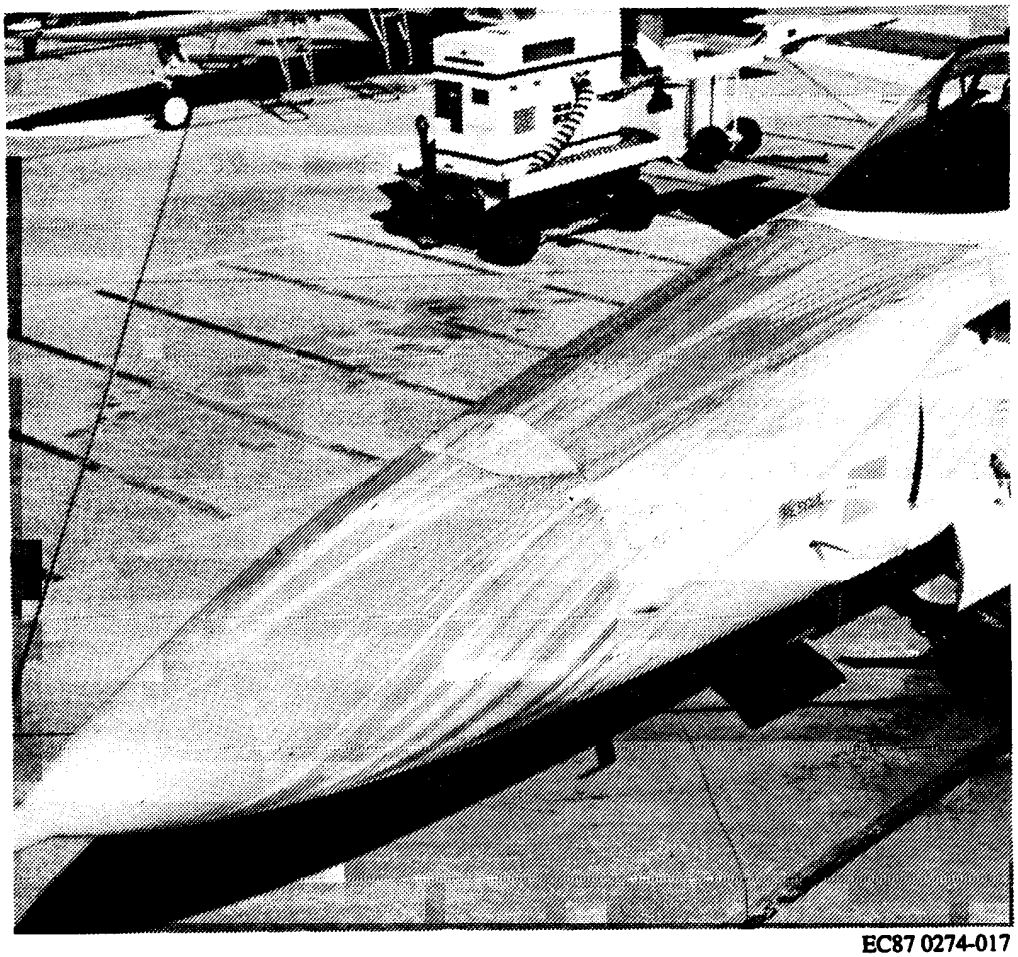

EC87 0274-017

Fig. 12 Visualization of surface flow on F-18 forebody, $\alpha = 19°$.

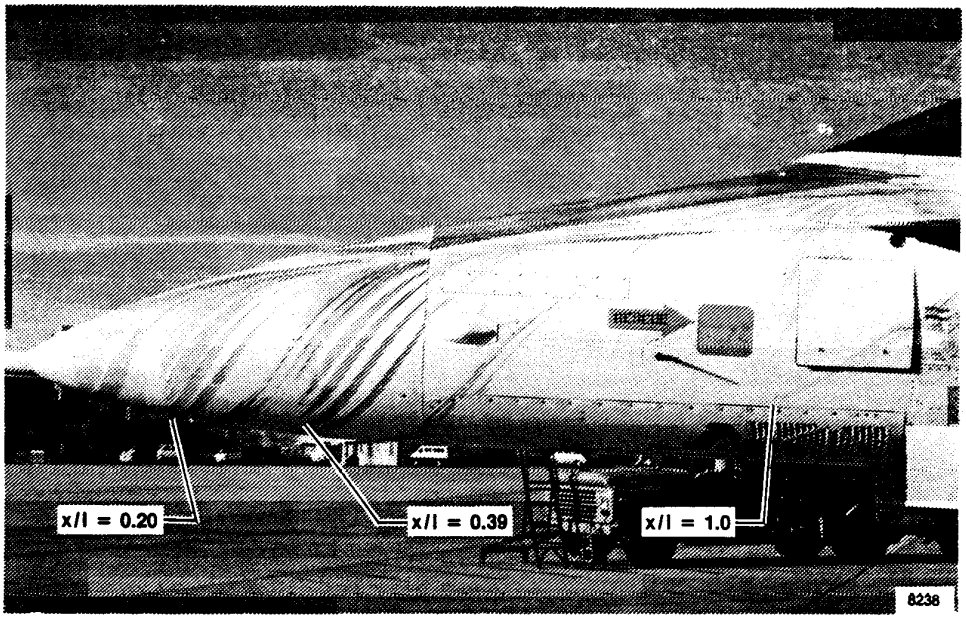

EC87 0277-004

(a) Surface streamlines on forebody.

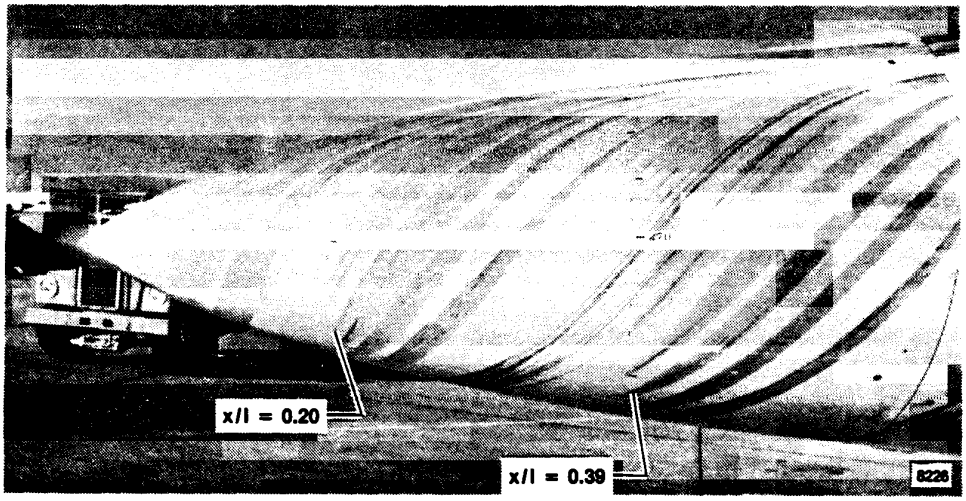

EC87 0277-009

(b) Surface streamlines on nose.

Fig. 13 Side view of F-18 forebody, $\alpha = 34°$.

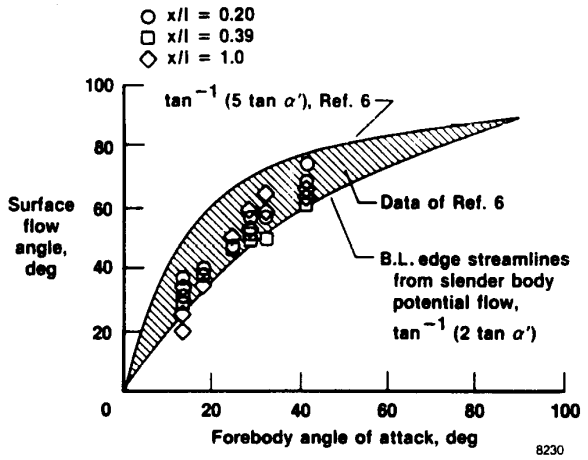

Fig. 14 Effect of forebody angle of attack on surface flow angle.

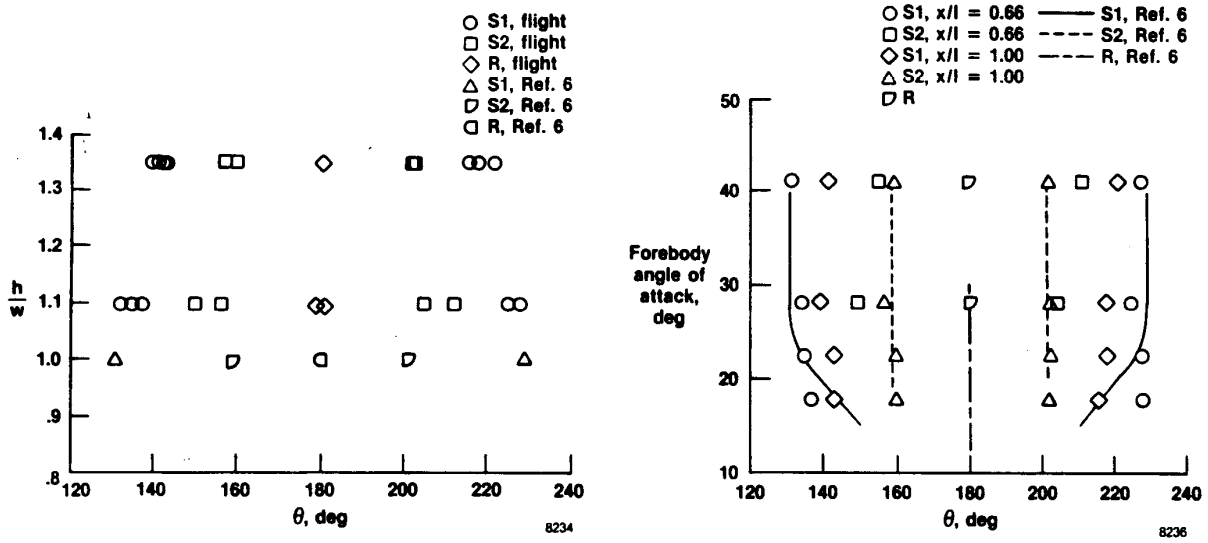

(a) As a function of h/w.

(b) As a function of forebody angle of attack.

Fig. 15 Locations of separation lines from flight and wind tunnel results.

NASA
National Aeronautics and Space Administration

Report Documentation Page

1. Report No.	2. Government Accession No.	3. Recipient's Catalog No.
NASA TM-100436		

4. Title and Subtitle

Surface Flow Visualization of Separated Flows on the Forebody of an F-18 Aircraft and Wind-Tunnel Model

5. Report Date

May 1988

6. Performing Organization Code

7. Author(s)

David F. Fisher, David M. Richwine, and Daniel W. Banks

8. Performing Organization Report No.

H-1481

10. Work Unit No.

RTOP 505-68-71

9. Performing Organization Name and Address

NASA Ames Research Center
Dryden Flight Research Facility
P.O. Box 273, Edwards, CA 93523-5000

11. Contract or Grant No.

13. Type of Report and Period Covered

Technical Memorandum

12. Sponsoring Agency Name and Address

National Aeronautics and Space Administration
Washington, DC 20546

14. Sponsoring Agency Code

15. Supplementary Notes

Prepared as AIAA88-2112 for presentation at the 4th Flight Test Conference, San Diego, California, May 18–20, 1988.

16. Abstract

A method of in-flight surface flow visualization similar to wind-tunnel-model oil flows is described for cases where photo-chase planes or onboard photography are not practical. This method, used on an F-18 aircraft in flight at high angles of attack, clearly showed surface flow streamlines on the fuselage forebody. Vortex separation and reattachment lines were identified with this method and documented using postflight photography. Surface flow angles measured at the 90° and 270° meridians, show excellent agreement with the wind tunnel data for a pointed tangent ogive with an aspect ratio of 3.5. The separation and reattachment line locations were qualitatively similar to the F-18 wind-tunnel-model oil flows but neither the laminar separation bubble nor the boundary-layer transition on the wind tunnel model were evident in the flight surface flows. The separation and reattachment line locations were in fair agreement with the wind tunnel data for the 3.5 ogive. The elliptical forebody shape of the F-18 caused the primary separation lines to move toward the leeward meridian. Little effect of angle of attack on the separation locations was noted for the range reported.

17. Key Words (Suggested by Author(s))	18. Distribution Statement
Flow visualization High angle of attack In-flight surface flow Oil flows Vortex separation	Unclassified — Unlimited Subject category 02

19. Security Classif. (of this report)	20. Security Classif. (of this page)	21. No. of pages	22. Price
Unclassified	Unclassified	18	A02

NASA FORM 1626 OCT 86

**For sale by the National Technical Information Service, Springfield, VA 22161-2171.*